THE BREAKDOWN OF SYNCHRONIZATION AND SHADOWING IN COUPLED CHAOTIC SYSTEMS: ANALYSIS VIA THE SUBSYSTEM DECOMPOSITION

ERNEST BARRETO and PAUL SO
Department of Physics & Astronomy and
The Krasnow Institute for Advanced Study
Mail Stop 2A1
George Mason University
Fairfax, Virginia 22030 USA
E-mail: ebarreto@gmu.edu, paso@gmu.edu

We present a powerful method of analyzing coupled chaotic systems in terms of a "subsystem" decomposition based on unstable periodic orbits. We focus on two important phenomena that have received a great deal of attention: synchronization and shadowability. This formalism forms the foundation for discussing these subjects in systems of non-identical coupled elements without special symmetries or invariant manifolds.

1 Introduction

Systems of several interacting nonlinear elements present a very rich variety of behavior, and often such systems collectively give rise to novel dynamics that are not obviously attributable to the individual component parts themselves. In this review, we present a powerful method of analysis of such systems. In particular, we focus on two important phenomena that have received a great deal of attention: synchronization and shadowability. Our methods not only serve to elucidate the processes that give rise to and destroy these phenomena, but they form the foundation for discussing these subjects in systems of non-identical coupled elements without special symmetries or invariant manifolds.

The synchronization of coupled chaotic oscillators, a phenomenon first noticed many years ago[1,2,3] is most naturally described in terms of a synchronization manifold: when synchronized, the time evolution occurs on a restricted set embedded in the full state space. However, as the degree of coupling is decreased to zero, this invariant synchronization manifold is typically destroyed (unless the system has special symmetries), and the system gradually evolves into a completely unsynchronized state in which all the degrees of freedom of the individual component maps are realized. At each extreme, the dynamics can be understood in terms of the individual components. In between, however, the situation is more complicated. This is discussed in Section 3.

Shadowability is a more subtle and perhaps more troubling issue. In its

absence, the significance of numerically-generated solutions to the underlying equations is called into question: a long numerical trajectory may not correspond to *any* mathematically true solution. Since most nonlinear systems are intractable except by computer analysis, it is essential to have an understanding of what conditions lead to the breakdown of shadowing, and how these systems evolve as these conditions are approached. This is discussed for the case of coupled chaotic systems in Section 4.

We find that both these issues can be fruitfully studied by considering the evolution of the system's unstable periodic orbit structure as the coupling is varied. Accordingly, our methods do not make reference to special symmetries or rely on the presence of invariant manifolds, and thus they are applicable to coupled systems of *dissimilar* elements. We draw particular attention to this case, since it represents almost every experimental situation of interest: in practice, it is very difficult to prepare sets of truly identical oscillators in physical experiments, and in biological systems, natural oscillators occur with considerable variability (for example, note the large variety of different neurons in the brain).

2 Defining UPO Subsystems

We begin by describing a "subsystem" decomposition of a general unidirectionally coupled system of chaotic maps of the form [a]

$$\begin{cases} x \to f(x) \\ y \to G(x, y; c). \end{cases} \tag{14.1}$$

Systems such as Equation (14.1) are known in the mathematical literature as skew products or extensions. Here we assume that the coupling is such that at $c = 1$, the x and y dynamics are in a state of generalized synchrony (i.e., $y = \phi(x)$), [2,5,6] and that at $c = 0$, the x and y dynamics are chaotic and completely independent of one another. f and G may be of any dimension. For illustration and ease of presentation, we use in our discussion below the simplest case

$$G(x, y; c) = cf(x) + (1 - c)g(y) \tag{14.1}$$

and take f and g to be quadratic maps with different parameters. (Another simple option is to use dissimilar Hénon maps.) Our arguments are not specific to these choices.

The subsystem decomposition of Equation (14.1) is defined as follows. [7] First, enumerate the periodic orbits of f (the driver), assigning each an index

[a] It has been shown that unidirectionally coupled systems are locally equivalent to bidirectionally coupled systems. [4]

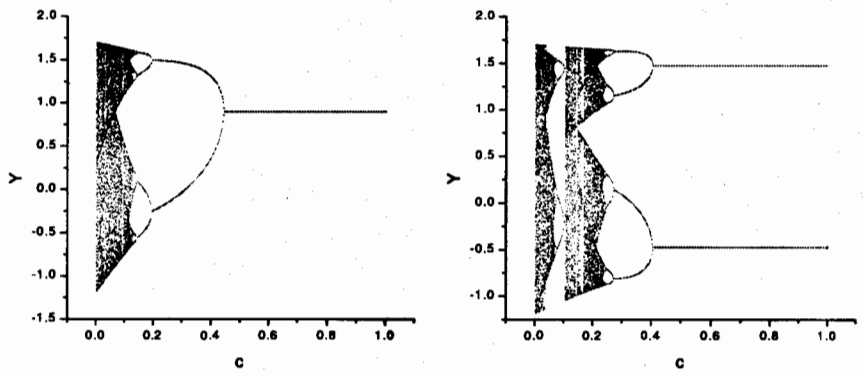

Figure 1: A subsystem consists of a drive-response coupled system, but with the drive fixed on one of its unstable periodic orbits. This figure shows bifurcation diagrams in the response variable of subsystems with (left) a period-1 and (right) a period-2 driver; the horizontal variable is the coupling.

$i = 1, 2, \ldots$. Then subsystem S_i is given by Equation (14.1), but with the driver dynamics, $f(x)$, locked on orbit i. We are interested in investigating the dynamics of individual subsystems. Note that because the driver is chaotic, an x-trajectory will come arbitrarily close to – and spend an arbitrarily long time near – any of the unstable periodic orbits embedded within its attractor. Thus, subsystem S_i contains the dynamics that the full-system trajectory experiences during close approaches to orbit i.

Figure 1 shows the bifurcation diagrams of a period-1 and a period-2 subsystem obtained from Equation (14.1) using $f = 1.7 - x^2$ and $g = 1.7 - y^2$. Figure 2 illustrates a period-4 subsystem from a four-dimensional version of Equation (14.1) using standard Hénon maps for f and g.

3 Desynchronization Beyond Generalized Synchrony

3.1 Introduction

We now address the issue of how synchronized chaotic systems desynchronize using the subsystem decomposition outlined above. Our goal is to analyze the evolution of the overall periodic orbit structure as the coupling is decreased and synchronization breaks down. We review two main results. [7] We describe the creation and evolution of a complicated set that develops outside of the synchronization manifold, which we call the *emergent set.* In addition, we quantitatively identify a critical transition point in its development; this we call

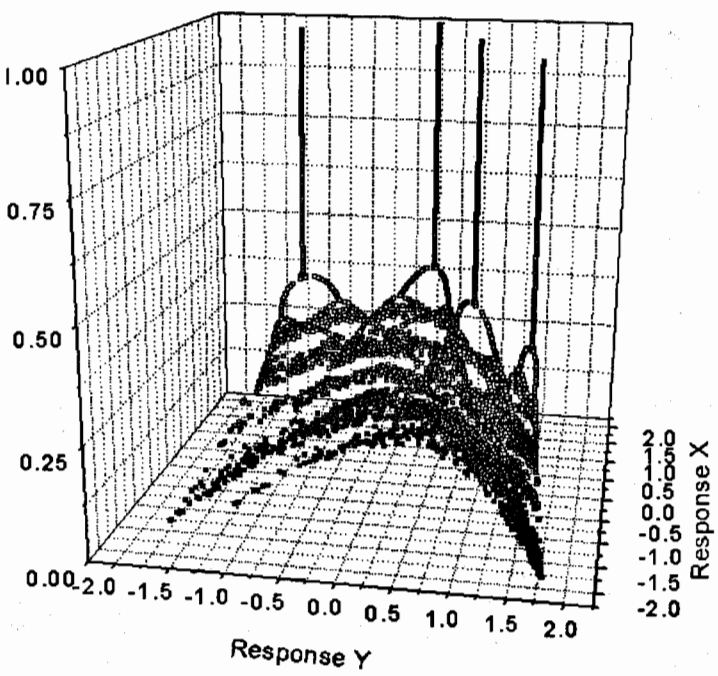

Figure 2: The bifurcation diagram for a subsystem drawn from a system of coupled Hénon maps. The driver is fixed on a period four orbit.

the *decoherence* transition. The identification of this transition is advantageous because it provides an experimentally measurable transition in situations where previously described bifurcation structures are inapplicable.

Previous work has focused on the invariant dynamics in a synchronization manifold $\mathcal{M}$, which can easily be identified in coupled systems with symmetry (such as when two identical sub-systems are coupled together). On $\mathcal{M}$, the components evolve identically, and are said to exhibit identical synchrony. [3] As the coupling decreases from a fully synchronized state, a bubbling bifurcation [8,9,10,11] occurs when an orbit within $\mathcal{M}$ (usually of low period [12]) loses transverse stability. In the presence of noise or *small* asymmetries, a typical trajectory quickly approaches and spends a long time in the vicinity of $\mathcal{M}$, but makes occasional excursions. (A related phenomenon is *riddling*. [13]) As the coupling is further decreased, the blowout bifurcation [14] is observed when

$\mathcal{M}$ itself becomes transversely unstable (on average). More recent work has described bifurcations that lead to the creation of periodic orbits off the synchronization manifold; [15] these may lead to the creation of chaotic attractors external to $\mathcal{M}$. [16] Also, imperfect phase synchrony has been analyzed recently in terms of unstable periodic orbits [17], and synchrony transitions have been investigated in coupled lattices of identical maps. [18]

The concept of (differentiable) generalized synchrony (GS) [2,5,6,19] extends these ideas. GS relaxes the condition that the state variables evolve identically, and only requires that they be functionally related. As the coupling is reduced and GS breaks down, however, this function may become extremely complicated, and the identification of bubbling-type or blowout-type bifurcations is especially problematic. Thus, a more general description of the desynchronization process is needed.

Here we extend the above description by considering the evolution of the unstable periodic orbits (UPOs) as the coupling is varied. In particular, we use Equation (14.1) and investigate this system as c is decreased from 1 to 0.

3.2 Evolution of the Attractor

The simplest case is when $f = g$, for which the synchronization manifold $\mathcal{M}$ (i.e. the line $x = y$) is invariant and attracting at $c = 1$. The bubbling bifurcation occurs when an orbit in $\mathcal{M}$ loses transverse stability, typically via a period-doubling (pitchfork) bifurcation. This leads to the creation of new orbits outside of $\mathcal{M}$. As the coupling is further reduced, more and more periodic orbits embedded in $\mathcal{M}$ lose their transverse stability in a similar fashion,[b] leading to the creation of additional orbits. As this process proceeds, the external UPOs simultaneously undergo period-doubling cascades to chaos, thus creating even more new orbits. We call the set of new orbits created in this fashion the *emergent set*.

In the more general case $f \neq g$, $x = y$ is by construction invariant and attracting for $c = 1$. Upon decreasing c, $x = y$ is no longer invariant, and we observe that the UPOs migrate and spread out as shown in Figure 3 for coupled quadratic maps. As the coupling is decreased, we first observe transverse Cantor-like structure, followed by a "fattening" of the striations as the Lyapunov dimension of the attractor increases to 2.0. [20,21] We have also observed similar UPO migration in the invertible case of coupled Hénon maps. It is remarkable that this UPO migration appears to occur well before any orbit loses its transverse stability. In fact, we observe a large range of c over which,

[b] Additional orbits external to $\mathcal{M}$ may be created by saddle-node bifurcation; these may then exchange stability with their corresponding orbits in $\mathcal{M}$ via a transcritical bifurcation.

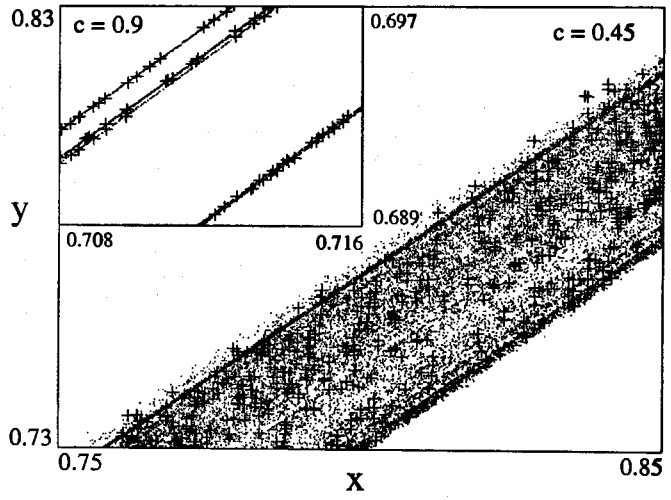

Figure 3: Magnifications of the attractor for Equation (14.1) with $f(x) = 1.7 - x^2$, $g(y) = 1.5 - y^2$, and $c = 0.45$ (inset, $c = 0.9$). Superimposed on both views are periodic orbits (+) of periods 1 to 20. At $c = 1$, these orbits lie on the diagonal $x = y$, but as c is decreased, they migrate as shown here. The Lyapunov dimension is 2.0 (inset, 1.25), and the orbits in both cases are transversely stable and one-to-one in the sense described in the text.

despite the apparent structure (ultimately two-dimensional), the periodic orbits migrate but are still transversely stable and one-to-one in the following sense: if the driver dynamics is fixed onto any one of its intrinsic period p orbits, then the limiting y dynamics is an attracting orbit *of the same period.*

Let U be the set of unstable periodic orbits on the line $x = y$ when $c = 1$. The number of orbits in U is determined by the driver and remains constant for all c because of the unidirectional coupling. For $f = g$, they remain fixed in place, but for $f \neq g$, they migrate as described above. As c is decreased from 1, the orbits' stability properties evolve, but they remain transversely attracting until a bubbling-type bifurcation is encountered. (We extend the concept of bubbling to the asymmetric case $f \neq g$ by defining it as the point where the first orbit in U loses stability[c]. As the coupling is further decreased, more and more orbits bifurcate and create orbits outside of U, and the above mechanism for the creation of the emergent set applies. Because of their migration, however, the orbits of U become intermingled among those of the emergent set.

[c]In all examples studied, the first such bifurcation is a period-doubling bifurcation.

3.3 *Subsystem Analysis*

We wish to view system (14.1) as an infinite collection of subsystems as defined in the previous section. To quantify the discussion, let $N_{xy}(p)$ denote the number of period p orbits of system (14.1). Also, let $N_f(p)$ denote the number of period p solutions of $f^p(x) - x = 0$ alone; $N_g(p)$ is defined analogously. These quantities contain contributions from all periodic orbits of period q, where q is an integer factor of p. For $c = 1$, the system exhibits identical synchrony and $N_{xy}(p) = N_f(p)$. In contrast, when $c = 0$, the system is fully decoupled into independent systems, and $N_{xy}(p) = N_f(p)N_g(p)$. (Note that $N_{xy}(p)$ may achieve its maximum at $c = 0$ or at intermediate values of c, depending on the nature of g.)

Our goal is to elucidate how this change in the unstable periodic orbit structure proceeds as c is varied. To this end, we consider the topological entropy h;[22] for large p, the number of periodic orbits of period p in a chaotic set increases exponentially with p as $N(p) \simeq e^{hp}$. Thus, the topological entropy of the coupled system is $h_{xy} = \lim_{p\to\infty} lnN_{xy}(p)/p$, and similarly, the topological entropy of the driver is $h_f = \lim_{p\to\infty} lnN_f(p)/p$.

Let $N_e(p)$ be the number of periodic orbits of period p that are not in U. These orbits reside in the emergent set and are created by the bifurcations described above. Thus $N_e(p) = \sum_{i=1}^{n_b} N_i(p)$, where the summation is over the number n_b of subsystems that have bifurcated. $N_i(p)$ is the number of periodic orbits of period p not in U that are associated with a particular subsystem S_i in the summation. The topological entropy of the emergent set is therefore $h_e = lim_{p\to\infty} N_e(p)/p$.[d]

We define the state of *topological coherence* for system (14.1) as the condition $h_{xy} = h_f$. In this state, the topological entropy of the system is determined by the driver. In order for topological coherence to be destroyed, the topological entropy of the full system h_{xy} must exceed h_f. This occurs when the emergent set becomes sufficiently complex. In the present case, $h_{xy} = \lim_{p\to\infty} \frac{1}{p} ln\left(N_f(p) + N_e(p)\right) = max(h_f, h_e)$. There is therefore a critical value c_d of coupling where h_e first exceeds h_f and topological coherence is lost. We call this the *decoherence transition.* For the special case $f = g$, we find that this typically occurs between the bubbling c_{bu} and the blowout c_{bo} bifurcations.

[d]Two scenarios lead to positive h_e: (1) $N_i(p)$ grows exponentially with p for a particular i, and (2) n_b grows exponentially with the period of the subsystem's driver.

3.4 *Measuring the decoherence transition from trajectory data*

We now address the question of how the decoherence transition may be measured from experimental data. First, we observe that in the symmetric noise-free case ($f = g$), trajectories collapse onto $\mathcal{M}$ and remain there until the blowout bifurcation. Thus, estimates of the decoherence transition based on measured data will not reflect the contribution of the emergent set. However, this case is exceptional. In the more general asymmetric case ($f \neq g$), the orbits of U migrate and become intermingled with those of the emergent set. Because of this, typical trajectories do not necessarily remain near U; instead, the observed attractor incorporates *parts* of the emergent set. How much of the emergent set is incorporated depends on the degree of asymmetry and the coupling. By using trajectory data, an *effective decoherence transition* can be measured which indicates how much the emergent set actually influences the observed dynamics. It is precisely this effective transition that is most relevant to the observed dynamics of the system and hence is most relevant to experimental situations. Below we describe an efficient method for estimating the effective decoherence transition that is based on actual trajectory information.

We use the methods of Jacobs, Ott, and Hunt. [26] These authors define an average n-step stretching rate as follows. Let $\lambda_i^{(n)}$ denote the square root of the largest eigenvalue of $[\mathbf{J}^n(\mathbf{x}_i)]^T\mathbf{J}^n(\mathbf{x}_i)$ for some initial condition $\mathbf{x}_i$, where $\mathbf{J}$ is the Jacobian of the system in Equation (14.1). Then form the following average quantity over m initial conditions chosen with respect to the natural measure: $ln\langle 1d\rangle_{n,m} = ln\left(\sum_{i=1}^{m}\lambda_i^{(n)}/m\right)/n$. For hyperbolic systems with one stretching direction, it can be shown [23,24,25,26] that $h_1 = \lim_{n\to\infty}\lim_{m\to\infty} ln\langle 1d\rangle_{n,m}$ is the topological entropy of the system[e]. Numerically, h_1 can be obtained by measuring the scaling of $ln(\sum_{i=1}^{m}\lambda_i^{(n)})$ with n, for a sufficiently large m.

Since Equation (14.1) can exhibit two expanding directions for certain parameter values, we also measure the two dimensional average stretching rate: $ln\langle 2d\rangle_{n,m} = ln\left(\sum_{i=1}^{m}(\lambda_1\lambda_2)_i^{(n)}/m\right)/n$, where $(\lambda_1\lambda_2)_i^{(n)}$ represents the square root of the product of the two largest eigenvalues of $[\mathbf{J}^n(\mathbf{x}_i)]^T\mathbf{J}^n(\mathbf{x}_i)$. The topological entropy when there are two expanding directions is given by $h_2 = \lim_{n\to\infty}\lim_{m\to\infty} ln\langle 2d\rangle_{n,m}$.

These quantities enable us to calculate the topological entropy of the full system as the coupling parameter varies and traverses regions with one and two stretching directions: $h_{xy} = max(h_1, h_2)$. For the examples considered

[e] If the logarithm is taken *before* the average, the result is the Lyapunov exponent. The procedure used here has contributions from other structure in the finite-time Lypunov exponent distribution.

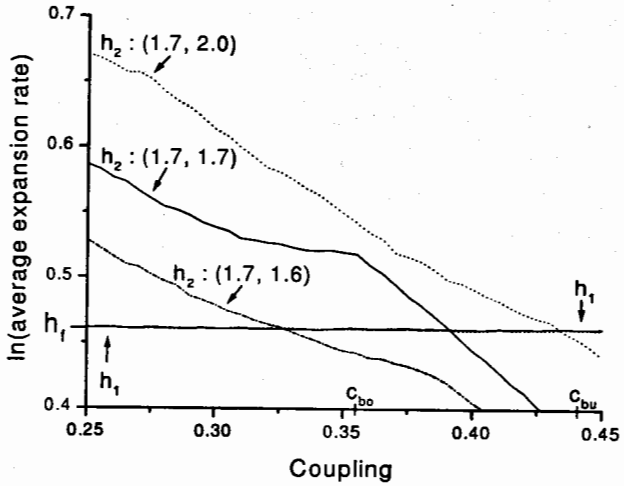

Figure 4: Topological entropy estimate $max(h_1, h_2)$ for the system in Equation (14.1) with $f(x) = 1.7 - x^2$, $g(y) = a_g - y^2$, and cases $a_g = 2.0$, 1.7, and 1.5. h_1 in all cases equals h_f, the topological entropy of the driver, for the range of coupling shown. The effective decoherence transition occurs when h_2 first exceeds h_1 (arrows). (For the symmetric case $a_g = a_f = 1.7$, bubbling occurs at $c_{bu} \simeq 0.442$ and blowout at $c_{bo} \simeq 0.352$.)

below, we have $h_1 = h_f$ for the entire coupling range of interest. Thus, the *effective* decoherence transition occurs when h_2 first exceeds $h_1 = h_f$. (In higher dimensional systems, these methods are practical if the number of unstable directions is low; otherwise, it may be difficult to accurately calculate these quantities from limited data. [27])

We apply these methods to a system of coupled quadratic maps. We take $f(x) = 1.7 - x^2$, $g(y) = a_g - y^2$, and consider the cases $a_g = 2.0$, 1.7, and 1.5. (We have also used two Hénon maps coupled as in Eq. 14.1, and the results are qualitatively the same.) Figure 4 shows $max(h_1, h_2)$ for these cases. [f] In all cases, h_1 is equal to the topological entropy of the driver dynamics h_f (for $a_g = 2.0$, $h_1 > h_f$ only for $c < 0.1$, not shown). The effective decoherence transition occurs when h_2 exceeds h_1, as indicated by arrows.

3.5 *Noise*

Finally, we illustrate the influence of the emergent set for $a_f = a_g = 1.7$ with noise. As c is decreased from bubbling, the dynamics will make occasional

[f] Figure 4 was generated using DYNAMICS [28]

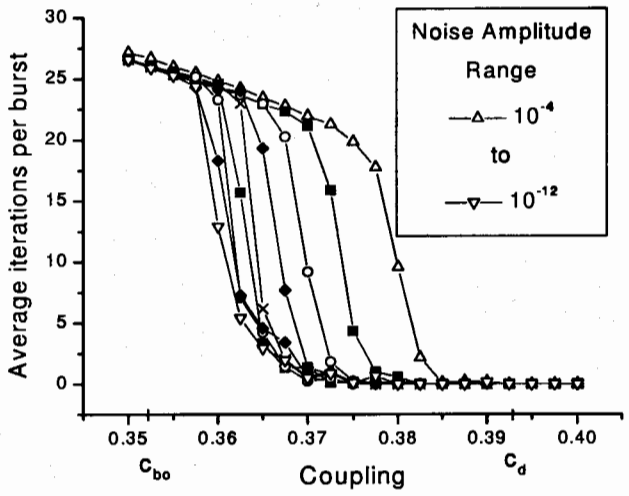

Figure 5: The duration of bursts away from the synchronization manifold for Equation (14.1) with $f(x) = 1.7 - x^2$ and $g(y) = 1.7 - y^2$. The threshold value of c for observing such bursts increases with larger noise. The curves asymptote to a common curve for coupling less than this threshold, indicating that the trajectory during the bursts is strongly influenced by the emergent set.

excursions from $\mathcal{M}$. We expect progressively longer transient times outside of $\mathcal{M}$ due to the increasing complexity of the emergent set. Figure 5 shows the average duration of a burst versus coupling. There is a transition range of c, (depending on noise) above which bursts are not observed. For small noise, this transition is close to the blowout; for larger noise, it shifts to higher coupling. Note that for c values below their respective transitions, the various curves asymptote to a common curve, suggesting that the dynamics during the bursts is consistently influenced by the emergent set. As expected, the average duration of bursts increases with decreasing c.

3.6 Conclusion

We conclude this section by emphasizing that the emergent set framework developed here is quite general and applies to coupled systems of non-identical elements where previously studied bifurcation structures may be inappropriate. Furthermore, the effective decoherence transition can be estimated in such systems from experimental data.

4 The Breakdown of Shadowing

4.1 Introduction

Nonlinear systems are frequently intractable, and therefore they are very often studied by numerical means and computer simulation. But because of the sensitivity to small errors that is inherent in chaotic systems, it is reasonable to question the validity of numerically-generated solutions to such systems. For example, round-off errors introduced at each step in a computer calculation may be so amplified by the dynamics inherent in the system being studied that the result is not useful.

A resolution to this problem is available for hyperbolic systems[29,30]. (Briefly stated, hyperbolic systems are ones for which the tangent space at each point can be split into clearly defined stable and unstable directions such that this splitting is preserved as the system evolves.) It can be shown that for such systems, there exist true trajectories which *shadow* numerical solutions. That is, given a computer-generated trajectory, there exists a mathematically-true solution, perhaps with a different initial condition, that remains close to the numerical solution. Thus, in this case, the results of computer simulations may be trusted. Similar results are also available for nearly hyperbolic systems.[31,32,33,34,35]

It is possible, however, for systems to be severely nonhyperbolic. One mechanism for this is unstable dimension variability (UDV). This refers to the presence of unstable periodic orbits (UPOs) with different numbers of unstable directions embedded within a chaotic attractor. Although first described long ago[36], interest in UDV and its consequences has grown recently,[37,38,39,40,41,42,43,44,45] especially since it was observed in a physically motivated model.[46] Severe UDV can cause very significant shadowing difficulties.[37] It has even been argued that systems that exhibit strong UDV may be, *in principle, deterministically unmodelable.*[42]

In this review we present a detailed analysis of the mechanisms that lead to the development of UDV as synchronized coupled chaotic systems desynchronize.[47] In addition, we quantify the degree of UDV as a function of coupling and find significant ranges of coupling where UDV is so severe that even very short numerically-generated trajectories are suspect. Again, we use Equation (14.1) with f and g being quadratic maps to illustrate our arguments.

4.2 Subsystem Analysis

As the coupling c is varied, each subsystem S_i exhibits an independent bifurcation structure in its y component. Each of these begin at $c = 1$ with x and

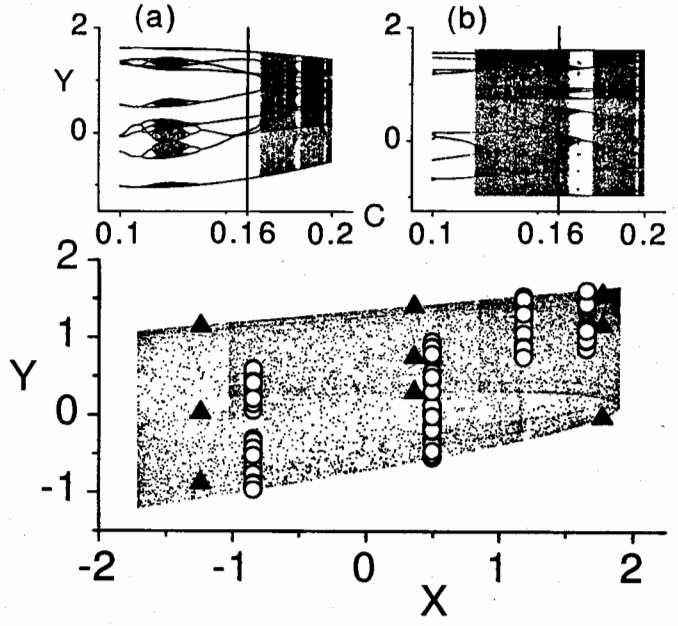

Figure 6: Unstable dimension variability for Equation (14.1) with $f(x) = 1.9 - x^2$ and $g(y) = 1.6 - y^2$. The panels show partial bifurcation diagrams of subsystems with (a) a period-3 and (b) a period-4 driver. The vertical lines are placed at $c = 0.16$, at which (a) exhibits an attracting period-9 orbit, and (b) exhibits chaos. The bottom panel shows the overall xy attractor at $c = 0.16$ with the subsystem dynamics superimposed. Triangles denote a period-9 saddle corresponding to (a), and circles denote an infinite number of repellers corresponding to (b).

y synchronized at the driving periodic orbit and progress (via period-doubling sequences, etc.) to the chaotic dynamics of g at $c = 0$. To illustrate, let $f(x) = 1.9 - x^2$ and $g(y) = 1.6 - y^2$, both of which are chaotic. The top panels in Figure 6 show partial bifurcation diagrams of subsystems that are driven by a period three and a period four driver. A vertical line is superimposed on each Figure at $c = 0.16$. At this particular coupling value, the period-3 subsystem (a) exhibits an attracting periodic orbit (of period 9), while the period-4 subsystem (b) exhibits chaos. The bottom panel shows the attractor for the overall coupled system. The asymptotic trajectories of the period-3 and period-4 subsystems are superimposed with triangles and circles, respectively.

We now argue that UDV is present in the example considered above, with $c = 0.16$. The period-3 subsystem is a periodically forced one-dimensional quadratic map in the y variable. For $c = 0.16$, it has an attracting period-9 orbit q whose stable set is an interval I_q in y (approximately $[-2, 2]$; compare scales in Figure 6). Viewed as an orbit of the original coupled map, Eq. 14.1, q is a *saddle* UPO. In particular, it has one stable direction along y, since its corresponding subsystem is attracting, and one unstable direction (with a non-zero projection along x), since f is chaotic. Correspondingly, the period-4 subsystem with $c = 0.16$ has a one-band chaotic attractor A in y whose stable set I_A is also an interval in y (again, approximately $[-2, 2]$). From similar arguments we conclude that A is a chaotic saddle of Eq. 14.1 and thus contains a dense set of *repellers* with two unstable directions (this is the one-dimensional version of the situation described in.[38,41])

Viewed in the full space of Eq. 14.1, the stable sets of q and A take on an additional complication. That is, the stable set of q (A) is the direct product of the set of preimages of the driving period-3 (4) orbit and the union of the appropriate preimages of I_q (I_A)[g]. Both these stable sets intersect the full attractor (compare I_q and I_A to Figure 6), and thus both q (saddle UPO) and A (containing repeller UPOs) are embedded within it.

Finally, we argue that q and A are recurrently connected in the sense of Ref. [38,41]. From the previous discussion, the stable sets of q and A are at least one dimensional since they contain a collection of intervals. Furthermore, the unstable sets of q and A are also at least one-dimensional, as can be seen by considering the evolution of a small interval in x centered around either q or a repeller within A. Because two lines generically intersect in two dimensions, we conclude that the stable set of q intersects the unstable set of A and that the unstable set of q intersects the stable set of A. These intersections are

[g]The preimages of I_q (or I_A) must be defined in terms of a sequence of maps $\{g_j\}$, where g_0 is the period-3 (4) subsystem and g_j is the response system driven by the jth preimage of the orbit that drives g_0.

Driver Period	Lyapunov exponent	Driver Period	Lyapunov exponent
1	−0.038	6	−0.394, **0.171**
2	**0.185**	7	−0.145, **0.176**
3	−0.363	8	−0.306, **0.143**
4	**0.167**	9	−0.141, **0.103**
5	−0.014, **0.159**	10	−0.130, **0.187**

Table 14.1: Largest Lyapunov exponents of several subsystems with drivers of periods $1-10$ for $f(x) = 1.9 - x^2$, $g(y) = 1.6 - y^2$, and $c = 0.16$. A negative Lyapunov exponent implies the presence of a saddle UPO in the attractor; a positive exponent implies the presence of an infinite number of repeller UPOs.

typically not destroyed by small perturbations. Thus we expect trajectories to visit both q and A recurrently.

These arguments establish UDV for Eq. 14.1 with $c = 0.16$. Other subsystems can be used in a similar manner to establish the simultaneous presence of additional saddle and repeller UPOs in the attractor; see Table 14.1. We confirm the presence of UDV in the full two-dimensional system by observing that the second largest finite-time Lyapunov exponent fluctuates about zero (inset in Figure 7).

4.3 Mechanisms for the Development of UDV

We now use the subsystem decomposition of Equation (14.1) to elucidate two distinct mechanisms for the development of UDV as the coupling is varied from 1 to 0 and the system desynchronizes. According to the subsystem decomposition, we think of each subsystem as a separate chaotic system with its own bifurcation structure, but with all subsystems sharing the coupling c as the bifurcation parameter. For $c = 1$, the overall dynamics is (by construction) attracted to the diagonal $x = y$, and each subsystem S_i collapses onto an orbit of period equal to that of its driver orbit. As c is decreased, a bifurcation analogous to the bubbling transition occurs [h] At this critical value of coupling, one particular subsystem (typically with a low-period driver) undergoes a bifurcation which converts the previously stable orbit to an unstable one. When viewed as a UPO of the combined system, this orbit is unstable in both the x and y directions. This is the first repeller UPO to appear, and this bubbling-like transition marks the first appearance of UDV.

[h] As described in Section 3, we extend the concept of bubbling to the asymmetric case $f \neq g$ by defining it as the point where the first subsystem bifurcation occurs.

As c is further decreased, other subsystems undergo similar bifurcations that create additional repellers. Meanwhile, the unbifurcated subsystems contribute saddle UPOs to the overall attractor. This is the first mechanism for the development of UDV. If the coupled system possesses an inherent symmetry, as when the coupled elements are identical, all of these orbits reside on an invariant synchronization manifold that contains the overall attractor; this is essentially the case studied in Refs. [42,43]. Our subsystem analysis, however, is not restricted to systems with such symmetries. More importantly, we argue below that the dominant contribution to severe UDV comes from the set of new orbits created as the various subsystems bifurcate.

As c is further decreased, still more subsystems bifurcate as described above. Meanwhile, a second parallel mechanism proceeds: the new orbits that are created as each individual subsystem bifurcates (usually via period-doubling) undergo cascades of period-doublings to chaos, apparently independently of one another. This process creates a huge number of new saddle and repeller UPOs in the overall system. We call the set of new orbits created in this way the *emergent set*. For $f = g$, these orbits reside outside the attractor until the blowout bifurcation. [i] However, in the more general case $f \neq g$, the destruction of the synchronization manifold (present only at $c = 1$) leads to the incorporation of most of the emergent set into the attractor. [7] Thus, for $f \neq g$, the combination of the two mechanisms outlined above lead to a dramatic increase in UDV. We believe that UDV is most severe once the system has lost topological coherence [7] and the emergent set dominates the overall dynamics.

4.4 Breakdown of Shadowing is Common in Coupled Systems

We conjecture that there is a set $\mathcal{C}$ of positive Lebesgue measure consisting of coupling values c at which some subsystems exhibit attracting periodic orbits while *simultaneously* other subsystems exhibit chaos. At such values of $c \in \mathcal{C}$, one can deduce by the arguments above that the attractor of the coupled system exhibits UDV. This implies that UDV can and will be encountered *in practice* when studying generic coupled chaotic systems, and thus the potential for severe shadowing and/or modeling breakdown is an important consideration for researchers investigating such systems.

It is reasonable to expect that $\mathcal{C}$ has positive measure in light of the results of Refs. [48,49,50]. Jacobson [48] proved that in the quadratic family, the set of parameter values that give rise to chaos has positive measure. Thus, if we assume that at a particular fixed value of c, the various subsystems are in some sense at random positions in each of their respective bifurcation diagrams (as

[i] At the blowout bifurcation, the synchronization manifold becomes repelling, on average. [14]

numerical investigations suggest), then there is a positive probability that at least some subsystems exhibit chaos and thus contribute repellers to the overall attractor. On the other hand, Graczyk and Świątek [49] proved, also for the quadratic family, that windows (i.e. parameter intervals that yield periodic behavior) occur densely in the parameter space. Thus it is also reasonable to expect that for the same fixed value of c, at least some subsystems exhibit attracting periodic orbits and therefore contribute saddles to the overall attractor. It is generally believed that the results of Refs. [48,49] carry over to higher dimensional situations in sufficiently high dimensional parameter spaces. [50]

Our arguments in this work do not rely on any specific features of f and G, other than that they are chaotic and that they desynchronize as the coupling between them is reduced to zero. Thus, the mechanisms for the creation of UDV in coupled systems described here is very general. In the case of *bidirectionally* coupled chaotic systems, distinct subsystems cannot be easily defined. Nevertheless, mechanisms similar to those described here can be observed. [51] More specifically, as a bidirectionally coupled system desynchronizes, the unstable periodic orbits embedded in the synchronized chaotic attractor lose transverse stability, typically via period-doubling bifurcations (mechanism 1); simultaneously, the new orbits created in this fashion undergo their own period-doubling cascades to chaos (mechanism 2). In contrast to the unidirectional case, these bifurcation sequences do not proceed independently. Instead, they interfere with each other and can lead to attractor crises [22] in the overall system. For example, such crises may lead to the destruction of the chaotic attractor and its replacement by an attracting periodic orbit. (In this case, however, a non-attracting chaotic set would remain containing UDV.)

4.5 Quantifying UDV and Shadowing Times

In the following, we quantify the degree of UDV and measure its evolution as a function of coupling. We consider both system (14.1) and a bidirectionally coupled case. For the latter, we use $x \to (1-c)f(x) + cg(y)$ and take y as in Equation (14.1). To quantify UDV, a *contrast measure*, defined for orbits of a given fixed period, has been proposed. [44] Here, we use the methods of Sauer, Grebogi and Yorke [40] to estimate the expected shadowing time. In effect, this takes UPOs of all periods into account at once. More importantly, the expected shadowing time is a physically relevant quantity that estimates the limitations of computer-based calculations.

The authors of Ref. [40] use a random walk approach to model the distribution of point-wise shadowing distances, i.e., the point-wise distances from a numerically-generated trajectory to its corresponding mathematically-true

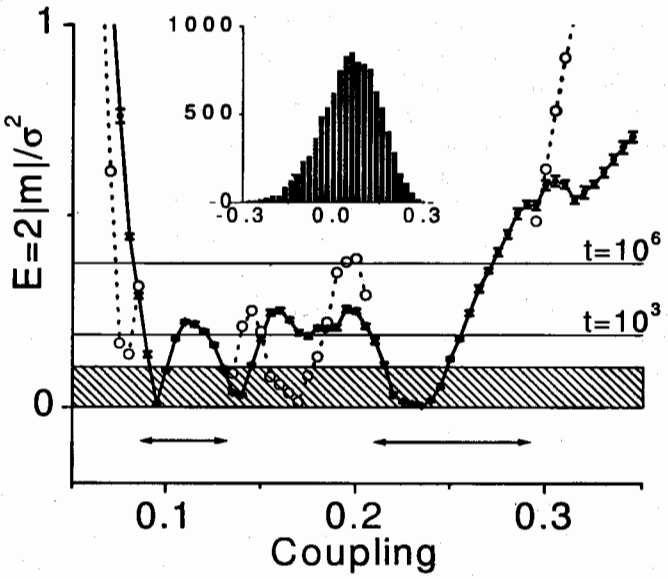

Figure 7: Shadowing time exponent E versus coupling (Inset: distribution of the time-50 Lyapunov exponent closest to zero for c=0.16, unidirectional case). The solid curve represents the unidirectionally coupled case; the dotted curve with circles is the bidirectionally coupled data. Horizontal lines indicate expected shadowing times of 10^6 and 10^3 iterations, assuming a calculational precision of 10^{-16}. Arrows indicate ranges of coupling values over which E is not graphed for the bidirectional case; see text.

"shadowing" orbit. The random walk, which includes a drift towards a reflecting barrier at the noise level, draws its parameters from the distribution of the finite-time Lyapunov exponent closest to zero. This is reasonable because the point-wise shadowing distance grows precisely when trajectories alternate between regions with different numbers of unstable directions. As the degree of UDV increases, such alternations occur more frequently. The expected shadowing time is calculated as the first-passage time for the shadowing distance to grow to the attractor size. In particular, the expected shadowing time may be estimated as 10^{pE}, where p is the number of digits of accuracy in the numerical computation and $E = \frac{2|m|}{\sigma^2}$. Here, m and σ^2 are the mean and variance of the distribution of the finite-time Lyapunov exponent closest to zero[j].

[j] The variance σ^2 is calculated using time-T Lyapunov exponents as $T\sigma_T^2$; we use $T = 50$. See Ref. [40].

Figure 7 shows the exponent E versus coupling for our two example systems, with $f(x) = 1.9 - x^2$ and $g(y) = 1.6 - y^2$. The horizontal lines correspond to expected shadowing times of 10^6 and 10^3 iterations, assuming a calculational accuracy of 10^{-16}. The solid curve represents the unidirectionally coupled case; the dotted curve with circles is the bidirectionally coupled data. In both cases, there is a significant range of coupling for which E is very small, thus indicating severe UDV and very short shadowing times. E is calculated using 10000 time-50 Lyapunov exponents at each value of coupling; error bars indicate the standard deviation of 20 measurements. The arrows indicate ranges of coupling values over which E is not graphed for the bidirectional case: within most of this range the system exhibits stable periodic behavior, and at the small-coupling end of the left arrow, these orbits period-double into a small two-piece chaotic attractor which explodes into the full attractor just below $c = 0.09$. The shaded region corresponds to shadowing times shorter than 50 iterations.

Finally, numerically-generated trajectories of systems with very short shadowing times may visit regions of the phase space with a frequency that is different from the system's true natural measure. Thus, infinite-time dynamical averages such as Lyapunov exponents, dimensions and entropies may not be accurate in such cases. To our knowledge there are no quantitative results linking expected errors for infinite-time averages to estimated shadowing times (related work is reported in. [45]) On the other hand, time-T averages for T less than the expected shadowing time (such as E values falling outside of the shaded box in Figure 7) should be reliable.

5 Conclusion

We have used the subsystem decomposition described in Section 2 to analyze both qualitatively and quantitatively the process whereby synchronized chaotic systems desynchronize, and how shadowing breaks down in such systems. These methods can serve as the foundation for discussing these subjects in systems of non-identical coupled elements without special symmetries or invariant manifolds.

Acknowledgments

This work was supported by the National Science Foundation (IBN 9727739) and the National Institutes of Health (2R01MH50006).

References

1. H. Fujisaka and T. Yamada, Prog. Theor. Phys. **69**, 32 (1983).
2. V.S. Afraimovich, N.N. Verichev, and M.I. Ravinovich, Izv. Vyssh. Uchebn. Zaved. Radiofiz. **29**, 1050 (1986) [Radiophys. Quantum Electron **29**, 795 (1986)].
3. L. M. Pecora and T. L. Carroll, Phys. Rev. Lett. **64**, 821 (1990).
4. K. Josić, Phys. Rev. Lett. **80**, 3053 (1998).
5. N. F. Rulkov, M. M. Sushchik, L. S. Tsimring, and H. D. I. Abarbanel, Phys. Rev. E **51**, 980 (1995).
6. L. Kocarev and U. Parlitz, Phys. Rev. Lett. **76**, 1816 (1996).
7. E. Barreto, P. So, B. J. Gluckman, and S. J. Schiff, Phys. Rev. Lett. **84**, 1689 (2000).
8. P. Ashwin, J. Buescu and I. Stewart, Phys. Lett. A **193**, 126 (1994).
9. P. Ashwin, J. Buescu and I. Stewart, Nonlinearity **9**, 703 (1996).
10. S. C. Venkataramani, et al., Phys. Rev. Lett. **77**, 5361 (1996).
11. S. C. Venkataramani, B. R. Hunt, and E. Ott, Phys. Rev. E **54**, 1346 (1996).
12. B. R. Hunt and E. Ott, Phys. Rev. Lett. **76**, 2254 (1996).
13. J. C. Alexander *et al.*, Int. J. Bifurcation Chaos **2**, 795 (1992); E. Ott, J. C. Sommerer, J. C. Alexander, I. Kan, and J. A. Yorke, Phys. Rev. Lett. **71**, 4143 (1993); J. C. Sommerer and E. Ott, Nature (London) **365**, 136 (1993); Y. C. Lai *et al.*, Phys. Rev. Lett. **77**, 55 (1996).
14. E. Ott and J. C. Sommerer, Phys. Lett. A 188, 39 (1994).
15. V. Astakhov, A. Shabunin, T. Kapitaniak and V. Anishchenko, Phys. Rev. Lett. **79**, 1014 (1997).
16. Yu. L. Maistrenko, V. L. Maistrenko, O. Popovych and E. Mosekilde, Phys. Rev. E **60**, 2817 (1999).
17. M. A. Zaks, E.-H. Park, M. G. Rosenblum, and J. Kurths, Phys. Rev. Lett. **82**, 4228 (1999).
18. See, for example, W. Just, Physica D **81**, 317 (1995) and references therein.
19. B. R. Hunt, E. Ott and J. A. Yorke, Phys. Rev. E **55**, 4029 (1997).
20. Similar behavior has been reported in Langevin-type dynamical systems; see C. Beck, Physica A **233**, 419 (1996).
21. V. Astakhov, T. Kapitaniak, A. Shabunin and V. Anishchenko, Phys. Lett. A **258** 99 (1999).
22. E. Ott, *Chaos in Dynamical Systems* (Cambridge University Press, Cambridge, England, 1993).
23. S. Newhouse, in Lecture notes in Physics Vol. 278 (Springer, Berlin,

1986), 2.
24. S. Newhouse, Ergod. Theor. Dynam. Syst. **8**, 283 (1988).
25. S. Newhouse and T. Pignataro, J. Stat. Phys. **72**, 1331 (1993).
26. J. Jacobs, E. Ott, and B. R. Hunt, Phys. Rev. E **57**, 6577 (1998).
27. J.-P. Eckmann and D. Ruelle, Physica D **56**, 185 (1992).
28. H. E. Nusse and J. A. Yorke, *Dynamics: Numerical Explorations* (Springer-Verlag, New York, Heidelberg, Berlin, 1994).
29. D. V. Anasov, Proc. Steklov Inst. Math. **90**, 1 (1967).
30. R. Bowen, J. Diff. Eqns. **18**, 333 (1975).
31. C. Grebogi, S. Hammel and J. A. Yorke, J. Complexity **3**, 136 (1987).
32. C. Grebogi, S. Hammel and J. A. Yorke, Bull. Am. Math. Soc. **19**, 465 (1988).
33. S-N. Chow and K. Palmer, Dynamics and Diff. Eqns. **3**, 361 (1991).
34. J. M. Sanz-Serna and S. Larsson, Appl. Num. Math. **13**, 181 (1993).
35. E. S. Van Vleck, SIAM J. Sci. Comput. **16** 1177 (1995).
36. R. Abraham and S. Smale, Proc. Symp. Pure Math. **14**, 5 (1970).
37. S. Dawson, C. Grebogi, T. Sauer, and J. A. Yorke, Phys. Rev. Lett. **73**, 1927 (1994).
38. S. P. Dawson, Phys. Rev. Lett. **76**, 4348 (1996).
39. E. J. Kostelich, I. Kan, C. Grebogi, E. Ott, and J. A. Yorke, Physica D **109**, 81 (1997).
40. T. Sauer, C. Grebogi, and J. A. Yorke, Phys. Rev. Lett. **79**, 59 (1997).
41. P. Moresco and S. P. Dawson, Phys. Rev. E **55**, 5350 (1997).
42. Y.-C. Lai and C. Grebogi, Phys. Rev. Lett. **82**, 4803 (1999).
43. Y.-C. Lai, D. Lerner, K. Williams, and C. Grebogi, Phys. Rev. E **60**, 5445 (1999).
44. Y.-C. Lai, Phys. Rev. E **59**, R3807 (1999).
45. Y.-C. Lai, C. Grebogi, and J. Kurths, Phys. Rev. E **59**, 2907 (1999).
46. F. J. Romeiras, C. Grebogi, E. Ott, and W. P. Dayawansa, Physica D **58**, 165 (1992).
47. E. Barreto and P. So, to appear in Physical Review Letters.
48. M. V. Jacobson, Comm. Math. Phys. **81**, 39 (1981).
49. J. Graczyk and G. Świątek, Ann. of Math **146**, 1 (1997).
50. E. Barreto, B. R. Hunt, C. Grebogi, and J. A. Yorke, Phys. Rev. Lett. **78**, 4561 (1997).
51. V. Astakhov, A. Shabunin, T. Kapitaniak, and V. Anishchenko, Phys. Rev. Lett **79**, 1014 (1997).